

# Correlation-assisted phonon softening and the orbital-selective Peierls transition in VO<sub>2</sub>

Sooran Kim, Kyoo Kim, Chang-Jong Kang, and B. I. Min

*Department of Physics, PCTP, Pohang University of Science and Technology, Pohang, 790-784, Korea*

(Received 5 July 2012; published 6 May 2013)

To explore the driving mechanisms of the metal-insulator transition (MIT) and the structural transition in VO<sub>2</sub>, we have investigated phonon dispersions of rutile VO<sub>2</sub> (*R*-VO<sub>2</sub>) in the density functional theory (DFT) and the DFT+*U* (*U*: Coulomb correlation) band calculations. We have found that the phonon softening instabilities occur in both cases, but the softened phonon mode only in the DFT+*U* describes properly both the MIT and the structural transition from *R*-VO<sub>2</sub> to monoclinic VO<sub>2</sub> (*M*<sub>1</sub>-VO<sub>2</sub>). The present *ab initio* phonon dispersion calculations clearly demonstrate that the Coulomb correlation effect plays an essential role of assisting the Peierls transition in *R*-VO<sub>2</sub> and producing the spin-Peierls ground state in *M*<sub>1</sub>-VO<sub>2</sub>.

DOI: [10.1103/PhysRevB.87.195106](https://doi.org/10.1103/PhysRevB.87.195106)

PACS number(s): 63.20.D-, 71.10.Fd, 71.30.+h

## I. INTRODUCTION

Vanadium dioxide (VO<sub>2</sub>) is one of the most explored transition metal oxides due to its intriguing metal-insulator transition (MIT) and the concomitant structural transition upon cooling. At ambient pressure and high temperature, VO<sub>2</sub> has a tetragonal rutile-type structure (*R*-VO<sub>2</sub>) with metallic nature. Upon cooling below 340 K, *R*-VO<sub>2</sub> undergoes the structural transition to a monoclinic structure (*M*<sub>1</sub>-VO<sub>2</sub>) with insulating nature.<sup>1,2</sup> The mechanism of MIT in VO<sub>2</sub> has been a longstanding subject of controversy. In the structural transition from *R*-VO<sub>2</sub> to *M*<sub>1</sub>-VO<sub>2</sub>, V ions construct the dimerization and the zigzag distortion. In *R*-VO<sub>2</sub>, V ions are centered at the distorted O<sub>6</sub> octahedra, which are edge-shared along the *c* axis. Due to the crystal field, V 3*d* states are split into *a*<sub>1*g*</sub> (*d*<sub>||</sub>), *e*<sub>*g*</sub><sup>π</sup> (*π*\*), and *e*<sub>*g*</sub><sup>σ</sup> states in order of energy, and so one electron of V<sup>4+</sup> ion occupies the lowest *a*<sub>1*g*</sub> state. While the zigzag distortion increases the energy of *e*<sub>*g*</sub><sup>π</sup> bands, the dimerization of V-V causes the splitting of *a*<sub>1*g*</sub> bands to open the gap at the Fermi level (*E*<sub>*F*</sub>).<sup>3</sup> This kind of structural distortion is explained by a typical Peierls transition.

However, the density functional theory (DFT) band approach fails to describe the insulating nature of *M*<sub>1</sub>-VO<sub>2</sub> properly.<sup>3–5</sup> The energy gap at *E*<sub>*F*</sub> can be obtained only when the extra Coulomb correlation *U* effect of V 3*d* electrons is considered, which indicates that *M*<sub>1</sub>-VO<sub>2</sub> is a Mott-Hubbard type insulator. Hence the Mott-Hubbard transition was proposed as the mechanism of MIT in VO<sub>2</sub>.<sup>6–8</sup> Beyond the DFT band approach, the *GW*<sup>9–11</sup> or the hybrid functional band method<sup>12,13</sup> were employed to describe the insulating nature of *M*<sub>1</sub>-VO<sub>2</sub> properly. Also the dynamical mean-field theory (DMFT) approach attempted to explain the insulating nature of *M*<sub>1</sub>-VO<sub>2</sub> by considering the Mott-Hubbard *U* explicitly.<sup>5,14–18</sup> Recently, the ground states and the insulating gap of VO<sub>2</sub> were explained by the modified Becke-Johnson potential.<sup>19</sup> Therefore the consensus at the moment is that some amount of Coulomb correlation is necessary to describe the insulating nature of *M*<sub>1</sub>-VO<sub>2</sub>.<sup>20,21</sup> However, whether *R*-VO<sub>2</sub> is a strongly correlated system or whether the Coulomb correlation effect is necessary for the MIT has not been clarified yet, despite several existing studies using the DFT+*U*<sup>22,23</sup> and the DMFT.<sup>5,16,17,24</sup>

As described above, there have been extensive electronic structure studies on VO<sub>2</sub>. By contrast, there have been only

several phonon studies on VO<sub>2</sub>.<sup>25–29,32</sup> Especially, there has been neither experimental nor *ab initio* theoretical report on the phonon dispersion curve for VO<sub>2</sub> yet. Since the Peierls transition is closely related to the phonon softening instability, the study of phonon dispersions of VO<sub>2</sub> is expected to give a clue to understanding the mechanism of MIT in VO<sub>2</sub>.<sup>25,29–33</sup>

In this paper, we have revisited the MIT and the structural transition of VO<sub>2</sub> by investigating the phonon dispersions of *R*-VO<sub>2</sub> and *M*<sub>1</sub>-VO<sub>2</sub>. We have examined the *U* effect on the phonon properties within the DFT+*U*. In fact, the DFT+*U* provides the proper nonlocal static screening,<sup>15</sup> which is essential to produce the dimerized state in *M*<sub>1</sub>-VO<sub>2</sub> and thereby captures properly the ground-state physics of phonon properties in VO<sub>2</sub>. We have found that *R*-VO<sub>2</sub> is a strongly correlated system with *U* ≥ 4.0 eV, and the Coulomb correlation effect plays an essential role in the MIT and the structural transition from *R*-VO<sub>2</sub> to *M*<sub>1</sub>-VO<sub>2</sub>.

## II. COMPUTATIONAL DETAILS

For the electronic structure and phonon dispersion calculations, the pseudopotential band method and the supercell approach that are implemented in VASP<sup>34</sup> and PHONOPY<sup>35</sup> are used. The full-potential band method implemented in WIEN2K is also employed to double-check electronic structures and energetics.<sup>36</sup> In the supercell approach for the phonon calculation, the force constants are calculated for a supercell with small lattice displacements, by using the Hellmann-Feynman theorem.<sup>37</sup> The utilized exchange-correlation functional is the generalized gradient approximation (GGA). The adopted values of *U* and *J* in the DFT+*U* are 4.2 and 0.8 eV, respectively.<sup>5</sup> All the phonon calculations were carried out after the full relaxation of the volume and atomic positions.<sup>38</sup> The initial structural parameters of *R*-VO<sub>2</sub> and *M*<sub>1</sub>-VO<sub>2</sub> before the relaxation are taken from experiments by McWhan *et al.*<sup>30</sup> and Longo *et al.*,<sup>39</sup> respectively. After the full-relaxation, the *c/a* and the volume of *R*-VO<sub>2</sub> become smaller than those before the relaxation, and similarly, the volume of *M*<sub>1</sub>-VO<sub>2</sub> decreases by relaxation.<sup>40</sup> As shown below, the full relaxation is essential to get the insulating state of *M*<sub>1</sub>-VO<sub>2</sub> in the DFT.

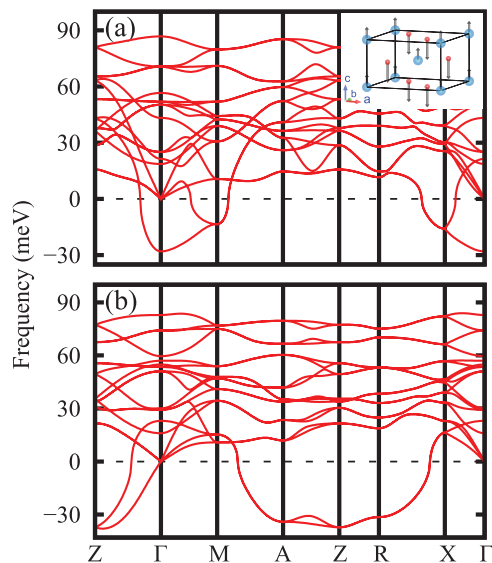


FIG. 1. (Color online) (a) The phonon dispersion curves of  $R\text{-VO}_2$  in the DFT. The inset shows the normal mode of softened phonon at  $\Gamma$ . (b) The phonon dispersion curves of  $R\text{-VO}_2$  in the DFT+ $U$ . Both figures show the negative phonon frequencies (imaginary frequencies) reflecting the phonon softening instability.

### III. RESULTS AND DISCUSSIONS

We have first obtained the electronic structures of  $R\text{-VO}_2$  in the DFT and the DFT+ $U$ . In the DFT, stable metallic states are obtained both in the nonmagnetic and the magnetic band structure calculations, in agreement with the experiment. However, in the DFT+ $U$ , a more stable insulating state is obtained in the magnetic band structure calculation, which is seemingly in disagreement with the experiment. In fact, the insulating state of  $R\text{-VO}_2$  in the DFT+ $U$  had been reported before.<sup>22,23</sup> This discrepancy between the calculation and the experiment can be resolved by considering the competition between the magnetic instability and the structural instability in  $R\text{-VO}_2$ . Of course, in nature, the structural instability wins over the magnetic instability, and so, upon cooling,  $R\text{-VO}_2$  undergoes the structural transition to  $M_1\text{-VO}_2$  in advance of the magnetic transition within  $R\text{-VO}_2$ .

Figure 1 shows the phonon dispersion curves of  $R\text{-VO}_2$  in the DFT and DFT+ $U$ . Four Raman modes ( $B_{1g}$ ,  $E_g$ ,  $A_{1g}$ , and  $B_{2g}$ ) are obtained in both cases, in agreement with experiments.<sup>26–28</sup> Interestingly, the phonon softening instabilities are obtained both in the DFT [see Fig. 1(a)] and in the DFT+ $U$  [see Fig. 1(b)], which imply that  $R\text{-VO}_2$  is not a stable structure. These results are expected because  $R\text{-VO}_2$  is stable only at high temperature. The most noteworthy is the marked difference in the phonon dispersion curves between the DFT and the DFT+ $U$ . In the DFT, the phonon softenings occur at  $\mathbf{q} = \Gamma$ ,  $M$ , and  $X$  [see Fig. 1(a)], while, in the DFT+ $U$ , they occur at  $\mathbf{q} = R$ ,  $A$ , and  $Z$  [see Fig. 1(b)]. The phonon softening at  $\mathbf{q} = R$  was once suggested to be responsible for the transformation from  $R\text{-VO}_2$  to  $M_1\text{-VO}_2$ .<sup>25,29–33</sup>

We have examined the normal modes of the softened phonons. The normal mode at  $\mathbf{q} = \Gamma$  in the DFT is plotted in the inset of Fig. 1(a), and those at  $\mathbf{q} = R$  in the DFT+ $U$  are plotted in Figs. 2(a) and 2(b). Recall that the main structural

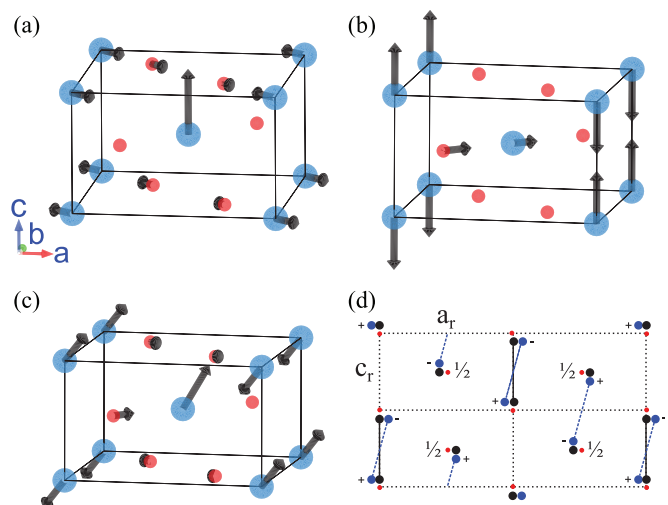


FIG. 2. (Color online) The normal modes of the softened phonons of  $R\text{-VO}_2$  in the DFT+ $U$  at  $\mathbf{q} = R$ . The blue and red balls represent V and O, respectively. There are two degenerate modes, as shown in (a) and (b). (c) A linearly superposed mode at  $\mathbf{q} = R$  using two degenerate modes of (a) and (b). (d) Schematic picture of V-V pairing and distortion in  $M_1\text{-VO}_2$ . Red, blue, and black dots denote V ions in  $R\text{-VO}_2$ ,  $M_1\text{-VO}_2$ , and  $M_2\text{-VO}_2$  (Cr-doped  $\text{VO}_2$  phase), respectively.

changes from  $R\text{-VO}_2$  to  $M_1\text{-VO}_2$  are the dimerization and zigzag distortion of V ions, as shown in Fig. 2(d). It is evident that those lattice distortions cannot be described by the normal mode at  $\Gamma$  in the DFT, which corresponds to just collinear displacements of ions along the  $c$  direction. The softened modes at  $M$  and  $X$  in the DFT do not describe the structural distortions either.<sup>40</sup> In contrast, the normal modes at  $R$  in the DFT+ $U$  are seen to be consistent with the lattice distortions of  $\text{VO}_2$ . As shown in Figs. 2(a) and 2(b), there are two degenerate softened phonon modes at  $R$ . The first mode in Fig. 2(a) represents the dimerizations of half of V ions and the orthogonal displacements of the other half. The second mode in Fig. 2(b) is just the reverse of the first one. Note that the mode predicted by Gervais *et al.*<sup>32</sup> is close to the first mode. Indeed, a linearly superposed mode using these two normal modes in Fig. 2(c) reveals simultaneous dimerizations and zigzag distortions of V ions, in perfect agreement with the observed lattice distortions in  $M_1\text{-VO}_2$  [see Fig. 2(d)]. The other independent superposed mode also reveals similar displacements of V ions. This agreement indicates that the softened mode at  $R$  in the DFT+ $U$  describes the structural transition of  $\text{VO}_2$  properly. The softened modes at  $A$  and  $Z$  in the DFT+ $U$  are also related to the dimerizations of V ions, but not directly to the zigzag distortions of V ions.<sup>40</sup>

The distinct phonon properties between the DFT and the DFT+ $U$  clearly demonstrates that the Coulomb correlation in  $R\text{-VO}_2$  facilitates the Peierls-type structural transition. Namely, in  $R\text{-VO}_2$ , the Coulomb correlation effect and the Peierls distortion are mutually cooperating in driving the MIT and the structural transition. To examine the  $U$  effect in more detail, we have checked the phonon dispersion curves with varying  $U$ . With increasing  $U$ , we have found that the softenings that occur in the DFT at  $\mathbf{q} = \Gamma$ ,  $M$ , and  $X$  disappear, whereas the softening at  $\mathbf{q} = A$ ,  $R$ , and  $Z$  emerge for  $U \geq 4.0$  eV (the larger  $U$ , the more negative of the phonon

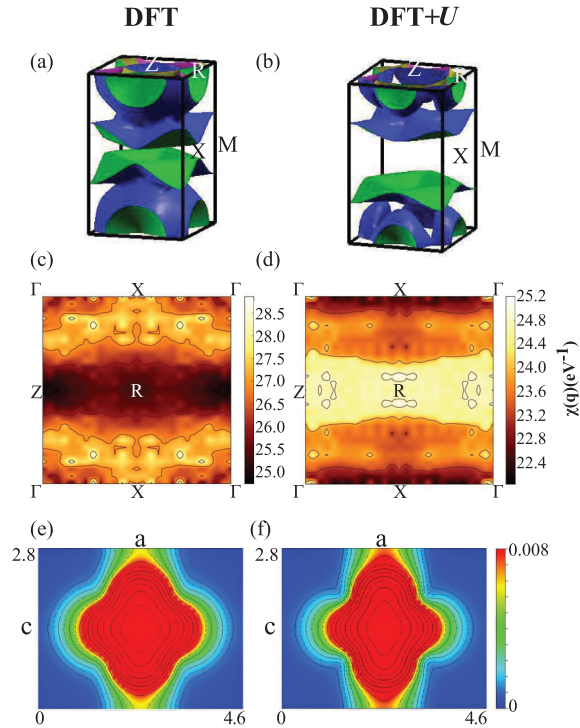


FIG. 3. (Color online) (a) and (b) The Fermi surface of  $R\text{-VO}_2$  in the DFT and in the DFT+ $U$ , respectively. (c) and (d)  $\chi(\mathbf{q})$  of  $R\text{-VO}_2$  in the DFT and in the DFT+ $U$ . (e) and (f) DFT and DFT+ $U$  local charge densities near  $E_F$  around the V ion of  $R\text{-VO}_2$  in the  $ac$  plane (integrated over  $\sim -1.2$  eV to  $E_F$ ) in  $\text{e}/\text{\AA}^3$  ( $x$  and  $z$  labels are in angstroms).

frequencies at  $\mathbf{q} = A, R,$  and  $Z$ ). This feature indicates that large enough  $U$  is required to produce the right Peierls distortions in  $\text{VO}_2$ . Below we analyze in more detail why the DFT and the DFT+ $U$  yield distinct phonon properties.

Figure 3 shows the Fermi surface, the electric susceptibility  $\chi(\mathbf{q})$ , and the local charge density of  $R\text{-VO}_2$  in the DFT and the DFT+ $U$  calculations. By comparing the Fermi surfaces in Figs. 3(a) and 3(b), one can notice that the Fermi surface becomes flatter in the DFT+ $U$ , suggesting a possible nesting effect along the  $c$  axis.<sup>41</sup> This change is more apparent in  $\chi(\mathbf{q})$ . As compared to  $\chi(\mathbf{q})$  in the DFT,  $\chi(\mathbf{q})$  in the DFT+ $U$  exhibits high values at  $\mathbf{q} = (x, 0, 0.5)$  ( $0 \leq x \leq 0.5$ ), which explains the origin of phonon softenings at  $\mathbf{q} = (x, 0, 0.5)$ , that is, at  $Z$  and  $R$  in Fig. 1(b). Local charge density plots in Figs. 3(e) and 3(f) also support the proper description of the DFT+ $U$  for the structural transition of  $R\text{-VO}_2$ . As compared to the case of the DFT, the charge density in the DFT+ $U$  is seen to be more anisotropic, reflecting that more charges are accumulated in the bonding region along the  $c$ -axis. This phenomenon arises from the correlation-induced orbital redistribution.

The partial density of states (PDOS) shown in Figs. 4(a) and 4(b) provides more clear evidence for the correlation-induced orbital redistribution. The orbital occupancies of  $a_{1g}(d_{x^2-y^2})$ ,  $e_g^\pi(d_{yz})$ , and  $e_g^\pi(d_{xz})$  in the DFT are in the ratio of 0.46, 0.32, and 0.22, whereas those in the DFT+ $U$  become 0.73, 0.14, and 0.13. Thus, due to  $U$  effect in  $R\text{-VO}_2$ , the occupancy of  $a_{1g}$  state is dramatically enhanced with respect to other  $e_g^\pi$  states, whereby the system becomes more one dimensional-

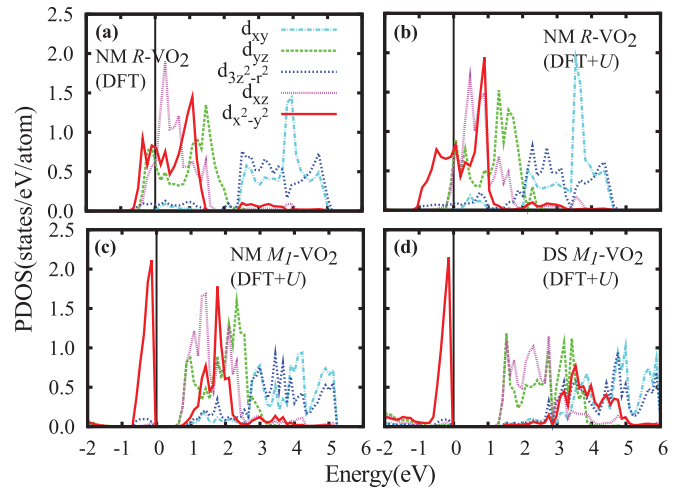


FIG. 4. (Color online) (a) The PDOS of the nonmagnetic (NM) state of  $R\text{-VO}_2$  in the DFT. (b) The PDOS of the NM state of  $R\text{-VO}_2$  in the DFT+ $U$ . (c) The PDOS of the NM state of  $M_1\text{-VO}_2$  in the DFT+ $U$ . (d) The PDOS of the dimerized-singlet (DS) state of  $M_1\text{-VO}_2$  in the DFT+ $U$ .

like along the  $c$  axis, and so more susceptible to the Peierls transition. Therefore, by means of the correlation-induced orbital redistribution, the orbital-selective Peierls transition occurs in the  $a_{1g}$  orbital. This feature is again consistent with the phonon softening in the DFT+ $U$  manifested at  $A, Z,$  and  $R$ , which are located in the  $z$  direction from  $\Gamma$ .

Now let us discuss the electronic structure of  $M_1\text{-VO}_2$ . In the nonmagnetic DFT calculation for  $M_1\text{-VO}_2$ , we have obtained the insulating state, even though the energy gap is very small ( $\sim 0.03$  eV).<sup>40</sup> This result is different from existing nonmagnetic DFT results in which metallic states were obtained for  $M_1\text{-VO}_2$ .<sup>3-5</sup> This difference is thought to come from the full relaxation of volume and ionic positions in our band calculations, which was not taken into account in the previous calculations. Without the relaxation, we also get the metallic state for  $M_1\text{-VO}_2$  in the nonmagnetic DFT calculation. On the other hand, in the nonmagnetic DFT+ $U$  calculation for  $M_1\text{-VO}_2$ , we have obtained the insulating state with large energy gap of  $\sim 0.67$  eV between  $a_{1g}$  and  $e_g^\pi$  states, as shown in Fig. 4(c), which appears to agree with the experimental gap of 0.6–0.7 eV.<sup>4,42</sup> It is clearly seen that the  $a_{1g}(d_{x^2-y^2})$  state is separated into bonding and antibonding states. We have calculated the phonon dispersions of  $M_1\text{-VO}_2$  both in the DFT and the DFT+ $U$  (not shown here). In both cases, there are no phonon softening instabilities. This indicates that  $M_1\text{-VO}_2$  is a stable ground-state structure, which is consistent with the experiment.

Note, however, the ground state of  $M_1\text{-VO}_2$  in the DFT+ $U$  is not the nonmagnetic state but the dimerized-singlet (DS) state, which has an antiferromagnetic spin configuration within each V-V dimer. The energy gap size of the DS state is obtained to be  $\sim 1.33$  eV, and the  $a_{1g}$  antibonding state is shifted further above, as shown in Fig. 4(d). The stable DS state is reminiscent of the spin-Peierls state, which has been suggested to be a ground state of  $M_1\text{-VO}_2$ .<sup>14,16,18,43-46</sup>  $M_1\text{-VO}_2$  has been considered to be a nonmagnet, because of the absence of magnetic response and magnetic order below

the MIT.<sup>47</sup> The absence of magnetic response in  $M_1$ -VO<sub>2</sub> can be understood by the spin-gap feature of the spin-Peierls state, as in other typical spin-Peierls systems, such as CuGeO<sub>3</sub><sup>48</sup> and NaV<sub>2</sub>O<sub>5</sub>.<sup>49</sup> In the DS state, the estimated spin-gaps amount to be  $\sim 0.32$  and  $\sim 0.38$  eV at the experimental and the theoretical equilibrium volumes, respectively.<sup>50</sup> Hence the spin-gap size depends slightly on the volume of the DS state, but it is much smaller than the charge-gap of 1.33 eV in Fig. 4(d). The obtained DS state with the different spin and the charge gaps supports that the ground state of  $M_1$ -VO<sub>2</sub> is the spin-Peierls state.

#### IV. CONCLUSION

Based on the phonon dispersion studies in the DFT and the DFT+ $U$ , we have demonstrated that the driving mechanism

of the MIT and the structural transition in VO<sub>2</sub> is the orbital-selective Peierls transition, subsequent to the correlation-induced orbital redistribution. The Coulomb correlation effect plays an essential role of assisting the Peierls transition in  $R$ -VO<sub>2</sub> and producing the spin-Peierls state in  $M_1$ -VO<sub>2</sub>. The phonon softening instability manifested at  $\mathbf{q} = R$  in the DFT+ $U$  provides direct evidence of Peierls mechanism of the structural transition from  $R$ -VO<sub>2</sub> to  $M_1$ -VO<sub>2</sub>.

#### ACKNOWLEDGMENTS

This work was supported by the NRF (Nos. 2009-0079947 and 2011-0025237), POSTECH Physics BK21 fund, and the KISTI supercomputing center (No. KSC-2012-C2-18). S.K. acknowledges the support from the NRF project of Global Ph.D. Fellowship (No. 2011-0002351).

- 
- <sup>1</sup>F. J. Morin, *Phys. Rev. Lett.* **3**, 34 (1959).  
<sup>2</sup>J. Goodenough, *Phys. Rev.* **117**, 1442 (1960).  
<sup>3</sup>V. Eyert, *Ann. Phys. (Leipzig)* **11**, 650 (2002).  
<sup>4</sup>R. M. Wentzcovitch, W. W. Schulz, and P. B. Allen, *Phys. Rev. Lett.* **72**, 3389 (1994).  
<sup>5</sup>A. Liebsch, H. Ishida, and G. Bihlmayer, *Phys. Rev. B* **71**, 085109 (2005).  
<sup>6</sup>A. Zylbersztein and N. F. Mott, *Phys. Rev. B* **11**, 4383 (1975).  
<sup>7</sup>T. M. Rice, H. Launois, and J. P. Pouget, *Phys. Rev. Lett.* **73**, 3042 (1994).  
<sup>8</sup>H.-T. Kim, Y. W. Lee, B.-J. Kim, B.-G. Chae, S. J. Yun, K.-Y. Kang, K.-J. Han, K.-J. Yee, and Y.-S. Lim, *Phys. Rev. Lett.* **97**, 266401 (2006).  
<sup>9</sup>A. Continenza, S. Massidda, and M. Posternak, *Phys. Rev. B* **60**, 15699 (1999).  
<sup>10</sup>M. Gatti, F. Bruneval, V. Olevano, and L. Reining, *Phys. Rev. Lett.* **99**, 266402 (2007).  
<sup>11</sup>R. Sakuma, T. Miyake, and F. Aryasetiawan, *Phys. Rev. B* **78**, 075106 (2008).  
<sup>12</sup>V. Eyert, *Phys. Rev. Lett.* **107**, 016401 (2011).  
<sup>13</sup>R. Grau-Crespo, H. Wang, and U. Schwingenschlöggl, *Phys. Rev. B* **86**, 081101(R) (2012).  
<sup>14</sup>S. Biermann, A. Poteryaev, A. I. Lichtenstein, and A. Georges, *Phys. Rev. Lett.* **94**, 026404 (2005).  
<sup>15</sup>M. S. Laad, L. Craco, and E. Müller-Hartmann, *Phys. Rev. B* **73**, 195120 (2006).  
<sup>16</sup>J. M. Tomczak, F. Aryasetiawan, and S. Biermann, *Phys. Rev. B* **78**, 115103 (2008).  
<sup>17</sup>B. Lazarovits, K. Kim, K. Haule, and G. Kotliar, *Phys. Rev. B* **81**, 115117 (2010).  
<sup>18</sup>A. S. Belozarov, M. A. Korotin, V. I. Anisimov, and A. I. Poteryaev, *Phys. Rev. B* **85**, 045109 (2012).  
<sup>19</sup>Z. Zhu and U. Schwingenschlöggl, *Phys. Rev. B* **86**, 075149 (2012).  
<sup>20</sup>M. W. Haverkort, Z. Hu, A. Tanaka, W. Reichelt, S. V. Streltsov, M. A. Korotin, V. I. Anisimov, H. H. Hsieh, H.-J. Lin, C. T. Chen, D. I. Khomskii, and L. H. Tjeng, *Phys. Rev. Lett.* **95**, 196404 (2005).  
<sup>21</sup>C. Weber, D. D. O'Regan, N. D. M. Hine, M. C. Payne, G. Kotliar, and P. B. Littlewood, *Phys. Rev. Lett.* **108**, 256402 (2012).  
<sup>22</sup>M. A. Korotin, N. A. Shorikov, and V. I. Anisimov, *Phys. of Metals and Metallograph (USSR)* **94**, 17 (2002).  
<sup>23</sup>G.-H. Liu, X.-Y. Deng, and R. Wen, *J. Mater. Sci.* **45**, 3270 (2010).  
<sup>24</sup>A. S. Belozarov, A. I. Poteryaev, and V. I. Anisimov, *JETP Lett.* **93**, 70 (2011).  
<sup>25</sup>J. R. Brews, *Phys. Rev. B* **1**, 2557 (1970).  
<sup>26</sup>R. Srivastava and L. Chase, *Phys. Rev. Lett.* **27**, 727 (1971).  
<sup>27</sup>P. Schilbe, *Physica B* **316–317**, 600 (2002).  
<sup>28</sup>P. Schilbe and D. Maurer, *Mater. Sci. Eng. A* **370**, 449 (2004).  
<sup>29</sup>C. J. Hearn, *J. Phys. C* **5**, 1317 (1972).  
<sup>30</sup>D. B. McWhan, M. Marezio, J. P. Remeika, and P. D. Dernier, *Phys. Rev. B* **10**, 490 (1974).  
<sup>31</sup>H. Terauchi and J. B. Cohen, *Phys. Rev. B* **17**, 2494 (1978).  
<sup>32</sup>F. Gervais and W. Kress, *Phys. Rev. B* **31**, 4809 (1985).  
<sup>33</sup>S. M. Woodley, *Chem. Phys. Lett.* **453**, 167 (2008).  
<sup>34</sup>G. Kresse and J. Furthmüller, *Phys. Rev. B* **54**, 11169 (1996); *Comput. Mater. Sci.* **6**, 15 (1996).  
<sup>35</sup>A. Togo, F. Oba, and I. Tanaka, *Phys. Rev. B* **78**, 134106 (2008).  
<sup>36</sup>P. Blaha, K. Schwarz, G. K. H. Madsen, D. Kvasnicka, and J. Luitz, WIEN2K (Karlheinz Schwarz, Technische Universität Wien, Austria, 2001).  
<sup>37</sup>K. Parlinski, Z. Q. Li, and Y. Kawazoe, *Phys. Rev. Lett.* **78**, 4063 (1997).  
<sup>38</sup>The selected  $\mathbf{k}$ -point samplings are  $6 \times 6 \times 10$  for  $R$ -VO<sub>2</sub> and  $6 \times 8 \times 6$  for  $M_1$ -VO<sub>2</sub> in the Monkhorst-Pack grid.  
<sup>39</sup>J. M. Longo and P. Kierkegaard, *Acta Chem. Scand.* **24**, 420 (1970).  
<sup>40</sup>See Supplemental Material at <http://link.aps.org/supplemental/10.1103/PhysRevB.87.195106> for relaxed structural parameters, normal modes of softened phonons, and DFT-DOS of  $M_1$ -VO<sub>2</sub>.  
<sup>41</sup>M. Gupta, A. J. Freeman, and D. E. Ellis, *Phys. Rev. B* **16**, 3338 (1977).  
<sup>42</sup>S. Shin, S. Suga, M. Taniguchi, M. Fujisawa, H. Kanzaki, A. Fujimori, H. Daimon, Y. Ueda, K. Kosuge, and S. Kachi, *Phys. Rev. B* **41**, 4993 (1990).  
<sup>43</sup>D. Paquet and P. Leroux-Hugon, *Phys. Rev. B* **22**, 5284 (1980).  
<sup>44</sup>J. Shi, R. Bruinsma, and A. R. Bishop, *Synth. Met.* **41–43**, 3527 (1991).  
<sup>45</sup>A. Cavalleri, M. Rini, and R. W. Schoenlein, *J. Phys. Soc. Jpn.* **75**, 011004 (2006).  
<sup>46</sup>T. C. Koethe, Z. Hu, M. W. Haverkort, C. Schüßler-Langeheine, F. Venturini, N. B. Brookes, O. Tjernberg, W. Reichelt, H. H. Hsieh, H.-J. Lin, C. T. Chen, and L. H. Tjeng, *Phys. Rev. Lett.* **97**, 116402 (2006).

- <sup>47</sup>J. P. Pouget, H. Launois, T. M. Rice, P. Dernier, A. Gossard, G. Villeneuve, and P. Hagenmuller, *Phys. Rev. B* **10**, 1801 (1974).
- <sup>48</sup>M. Hase, I. Terasaki, and K. Uchinokura, *Phys. Rev. Lett.* **70**, 3651 (1993).

- <sup>49</sup>M. Isobe and Y. Ueda, *J. Phys. Soc. Jpn.* **65**, 1178 (1996).

<sup>50</sup>The spin gap is approximately obtained by the energy difference between the singlet and triplet spin configurations in the V-V dimer. The total energy calculations were done by employing the WIEN2K code.